

Symmetry-protected adiabatic quantum metrology

Takuya Hatomura,^{1,*} Atsuki Yoshinaga,^{2,3,†} Yuichiro Matsuzaki,^{3,‡} and Mamiko Tatsuta^{3,§}

¹*NTT Basic Research Laboratories & NTT Research Center for Theoretical Quantum Physics, NTT Corporation, Kanagawa 243-0198, Japan*

²*Department of Physics, University of Tokyo, Chiba 277-8574, Japan*

³*National Institute of Advanced Industrial Science and Technology, Ibaraki 305-8568, Japan*

(Dated: April 8, 2021)

The aim of quantum metrology is to estimate target parameters as precisely as possible. In this paper, we propose a protocol for quantum metrology based on symmetry-protected adiabatic transformation. We introduce a ferromagnetic Ising model with a transverse field as a probe and consider the estimation of a longitudinal field. Without the transverse field, the ground state of the probe is given by the Greenberger-Horne-Zeilinger state, and thus the Heisenberg limit estimation of the longitudinal field can be achieved through parity measurement. We find that information of the longitudinal field encoded on parity can be mapped to global magnetization by symmetry-protected adiabatic transformation, i.e., parity measurement can be replaced with global magnetization measurement. Our scheme requires neither accurate control of individual qubits nor that of interaction strength.

I. INTRODUCTION

Precise estimation of parameters is desired for realizing upcoming quantum technologies such as quantum information processing. Quantum metrology is a promising method that offers higher precision sensing of target parameters than classical counterparts by exploiting entanglement [1–3]. Appropriate entanglement among probe qubits enhances sensitivity, surpassing the standard quantum limit (SQL) [4–6], which is known as the limit of classical sensors composed of separable states. In particular, the Greenberger-Horne-Zeilinger (GHZ) state [7, 8] achieves the ultimate precision called the Heisenberg limit in the absence of noise [9, 10]. Even under specific noise, the GHZ state can still beat the SQL [11–17]. Considerable effort has been devoted to the development of entanglement generation and interferometry for practical use. However, application of entanglement-enhanced sensing is still limited due to the following reasons.

One of the major challenges in entanglement-enhanced sensing is to develop robust schemes against experimental imperfection. Typically, entanglement is created by gate operations [18–24] or nonlinear interactions [25–32]. Controlled pulse sequences are required for adequately turning on/off gates or interactions to complete entanglement generation and to proceed to interferometry. It implies that complicated and precise setups are necessary in experiments. Desirable schemes should not require accurate control of (individual) qubits. Recently, such schemes using interacting systems have been proposed [33, 34]. In these schemes, interactions are not necessarily turned off.

In a ferromagnetic Ising model with a transverse field, macroscopic entanglement can be created in the ground state by adiabatically decreasing the transverse field [35–37]. This process does not require accurate control of qubits. Moreover, this process is protected by symmetry, i.e., nonadiabatic transitions from even-parity energy eigenstates to odd-parity energy eigenstates do not take place because of parity conservation based on spin-flip symmetry [38–40]. This suppression of nonadiabatic transitions protects the macroscopic entanglement from spontaneous symmetry breaking.

To use the macroscopic entanglement in the ferromagnetic Ising model for quantum metrology, parity measurement is required to extract information of a target parameter. Several ways to perform parity measurement exist. For example, we can obtain information of parity by post-processing data of single-qubit measurement on each qubit. However, operators to be measured in single-qubit measurement do not commute with the Hamiltonian (interaction term). In general, measurement of operators that do not commute with a given Hamiltonian is experimentally hard [41], and thus we cannot perform single-qubit measurement unless interactions are turned off.

In this paper, we propose a scheme for quantum metrology, in which we use the macroscopic entanglement in the ferromagnetic Ising model. In our scheme, after exposing the macroscopically entangled state to a target longitudinal field, we adiabatically induce the transverse field again. This process is also protected by the symmetry, conserving the parity. Consequently, we can extract information of the parity by global magnetization measurement. For the strong transverse field, an operator to be measured commutes with the dominant part of the Hamiltonian (transverse field term), and thus our scheme is feasible in experiments. Some realistic situations are also discussed.

* takuya.hatomura.ub@hco.ntt.co.jp

† a-yoshinaga@aist.go.jp

‡ matsuzaki.yuichiro@aist.go.jp

§ mamiko.tatsuta@aist.go.jp

II. THEORY

A. Parameter estimation

We express a probe state exposed to a target parameter θ with an unknown value during a time interval T_{int} as $|\Psi_{T_{\text{int}}}(\theta)\rangle$. When a readout process corresponds to projection measurement, uncertainty of the estimation is given by

$$\delta\theta = \frac{\sqrt{P(1-P)}}{\left|\frac{\partial P}{\partial\theta}\right| \sqrt{M}}, \quad (1)$$

where

$$P = \langle\Psi_{T_{\text{int}}}(\theta)|\hat{P}|\Psi_{T_{\text{int}}}(\theta)\rangle \quad (2)$$

with a projection operator \hat{P} denoting the survival probability and M denoting the number of measurement [2]. Since we are interested in scaling behavior of the uncertainty against the number of qubits, we set $M = 1$ throughout the paper for simplicity.

B. Model

Our theory can be applied to any ferromagnetic Ising model with a transverse field, but we focus on the following infinite-range Ising model with a transverse field

$$\hat{\mathcal{H}} = -\frac{1}{2}J \sum_{i,j=1}^N \hat{Z}_i \hat{Z}_j - h^x \sum_{i=1}^N \hat{X}_i, \quad (3)$$

where we express Pauli matrices as $\{\hat{X}, \hat{Y}, \hat{Z}\}$, and J and h^x are the interaction strength and the amplitude of the transverse field, respectively. We assume that h^x is tunable, while J is fixed. This is a reasonable assumption for many physical systems. In addition, we assume N to be even for simplicity. Our purpose is to estimate a target longitudinal field h^z . In a sensing process,

$$\hat{V} = -h^z \sum_{i=1}^N \hat{Z}_i \quad (4)$$

is added to the Hamiltonian (3).

For convenience, we use eigenvectors

$$\hat{S}_W |N/2, m\rangle_W = m |N/2, m\rangle_W \quad (W = X, Y, Z) \quad (5)$$

of collective spin operators

$$\hat{S}_W = \frac{1}{2} \sum_{i=1}^N \hat{W}_i \quad (W = X, Y, Z) \quad (6)$$

to express energy eigenstates of the Hamiltonian (3). Here we suppose that the system is confined in the maximum spin subspace satisfying $\sum_{W=X,Y,Z} \hat{S}_W^2 = N/2 \times (N/2 + 1)$, i.e., $m = -N/2, -N/2 + 1, \dots, N/2$.

This system (3) conserves the parity

$$\hat{\Pi} = \prod_{i=1}^N \hat{X}_i, \quad (7)$$

i.e., the commutation relation between the Hamiltonian (3) and the parity operator (7) becomes zero. That is,

$$[\hat{\mathcal{H}}, \hat{\Pi}] = 0 \quad (8)$$

for any h^x (see, e.g., Ref. [38–40]). Therefore, $(N+1)$ energy eigenstates of the Hamiltonian (3) in the maximum spin subspace are classified into two sets, $\{|\psi_n(h^x)\rangle\}_{n=0}^{N/2}$ with the parity $\hat{\Pi} = +1$ and $\{|\phi_n(h^x)\rangle\}_{n=0}^{N/2-1}$ with the parity $\hat{\Pi} = -1$, in the ascending order of energy, respectively. These energy eigenstates are given by

$$\begin{cases} |\psi_n(\infty)\rangle = |N/2, N/2 - 2n\rangle_X, \\ |\phi_n(\infty)\rangle = |N/2, N/2 - (2n+1)\rangle_X \end{cases} \quad (9)$$

in the $h^x \rightarrow \infty$ limit and

$$\begin{cases} |\psi_n(0)\rangle = \frac{1}{\sqrt{2}}(|N/2, N/2 - n\rangle_Z + |N/2, n - N/2\rangle_Z), \\ |\phi_n(0)\rangle = \frac{1}{\sqrt{2}}(|N/2, N/2 - n\rangle_Z - |N/2, n - N/2\rangle_Z), \end{cases} \quad (10)$$

for $n = 0, 1, \dots, N/2 - 1$ and $|\psi_{N/2}(0)\rangle = |N/2, 0\rangle_Z$ in the $h^x \rightarrow 0$ limit. Notably, the degenerate ground states $|\psi_0(0)\rangle$, which is known as the GHZ state, and $|\phi_0(0)\rangle$ as well can achieve the Heisenberg limit by parity measurement [9].

For example, we can obtain the expectation value of the parity (7) by implementing single-qubit measurement of \hat{X} on each qubit and multiplying the measurement outcomes, and by averaging it for many independent and identically distributed samples. However, single-qubit measurement of \hat{X} is nontrivial for the present model because each \hat{X} does not commute with the interaction term of the Hamiltonian. If the interaction term is much smaller than the resonant frequency of qubits, we can perform single-qubit rotation along the y -axis by $\pi/2$ and subsequent single-qubit measurement of \hat{Z} , which commutes with the interaction term of the Hamiltonian, for each qubit. The measurement outcome is equivalent to \hat{X} of the original state. However, when the interaction term is as large as or larger than the resonant frequency of qubits, we cannot use this method. Other approaches are necessary to measure the parity.

C. Symmetry-protected adiabatic quantum metrology

In this section, we explain our scheme with a reasonable readout protocol extracting information of the parity. First, we generate $|\psi_0(0)\rangle$ by adiabatic transformation, i.e., we prepare the trivial ground state $|\psi_0(\infty)\rangle$ as the initial state and adiabatically change the transverse field h^x from infinity to zero [35–37]. Notably, this process is protected by the parity conservation based on the spin-flip symmetry, i.e., nonadiabatic transitions from the ground state $|\psi_0(h^x)\rangle$ to the degenerate ground state $|\phi_0(h^x)\rangle$ do not take place even if the transverse field becomes small [38–40]. We then expose the system to the target longitudinal field h^z during a time interval T_{int} . Consequently, the state changes as

$$e^{-i(\hat{H} + \hat{V})T_{\text{int}}}|\psi_0(0)\rangle = e^{iJN^2T_{\text{int}}/2}[\cos(h^z NT_{\text{int}})|\psi_0(0)\rangle + i \sin(h^z NT_{\text{int}})|\phi_0(0)\rangle]. \quad (11)$$

In our scheme, we adiabatically change the transverse field h^x again to infinity. The state (11) becomes

$$|\Psi_{T_{\text{int}}}(h^z)\rangle = \cos(h^z NT_{\text{int}})|\psi_0(\infty)\rangle + \sin(h^z NT_{\text{int}})e^{i\alpha}|\phi_0(\infty)\rangle \quad (12)$$

except for a global phase factor because of the parity conservation (8). Here, α is a relative phase accompanying the adiabatic transformation of the transverse field h^x . To extract the information of the target longitudinal field h^z from this state, we perform projection measurement of the eigenstate $|\psi_0(\infty)\rangle = |N/2, N/2\rangle_X$. This measurement can simply be implemented by measuring the global magnetization \hat{S}_X , which commutes with the dominant part of the Hamiltonian (transverse field term). The expectation value of the projection measurement (2) is given by $P = \cos^2(h^z NT_{\text{int}})$, and thus the uncertainty of the estimation (1) achieves the Heisenberg limit

$$\delta h^z = \frac{1}{2NT_{\text{int}}}. \quad (13)$$

In conclusion, experimentally difficult parity measurement is replaced with simple global magnetization measurement, keeping the Heisenberg limit.

D. Phase shift

While the uncertainty achieves the Heisenberg limit even for vanishingly small h^z , both the denominator and the numerator in Eq. (1) vanish for $h^z \ll 1$ because the expectation value of the projection measurement (2) is the cosine-squared function. However, in noisy situations, the numerator typically has a finite value, while the denominator is infinitesimal for small h^z , resulting in divergence of the uncertainty. For example, the numerator becomes large when readout measurement becomes noisy [42, 43].

To avoid such a problem, we introduce a phase shift. The target parameter can be divided into two parts, $h^z = h_k^z + h_u^z$, where h_k^z is a known part and h_u^z is an unknown part. We assume that, by pre-estimation, an approximate value of h^z is known, i.e., $h_k^z \approx h^z$ and $h_u^z \ll 1$. We try to estimate h_u^z by entanglement-enhanced sensing for further improvement of precision. For a phase shift, we add an offset h_0^z so that $2(h_k^z + h_0^z)NT_{\text{int}} = (2n + 1)\pi/2$ with an integer n . Then, the expectation value of the projection measurement (2) turns into $P = [1 \pm \sin(2h_u^z NT_{\text{int}})]/2$, and thus the denominator of Eq. (1) does $|\partial P / \partial h^z| = NT_{\text{int}}|\cos(2h_u^z NT_{\text{int}})|$, which does not vanish for small h_u^z . Due to this phase shift, the uncertainty of the estimation (1) becomes robust against noise.

E. Realistic situation

We now consider a case, where the transverse field h^x and its transformation speed are finite in order to discuss a realistic situation in experiments. We set the transverse field h^x at the initial and final time as $h^x = h_0^x$, and assume that the transverse field is changed from $h_0^x(0)$ to 0 (h_0^x) with finite operation time T_a . For finite operation time, some nonadiabatic transitions may happen, but the parity conservation (8) guarantees that transitions between different parity eigenstates $\{|\psi_n(h^x)\rangle\}_{n=0}^{N/2}$ and $\{|\phi_n(h^x)\rangle\}_{n=0}^{N/2-1}$ do not take place as well as in the ideal situation [38–40].

Let us discuss two approaches to prepare the initial state. The first approach is as follows: for $h_0^x/JN \gg 1$, we prepare the ground state $|\psi_0(h_0^x)\rangle$ as the initial state, which can be done by cooling the system because of large energy gap. However, in this case, long operation time is required to adiabatically change the transverse field from large h_0^x to 0 and from 0 to large h_0^x . The other approach is as follows: we apply a strong magnetic field $h^x/JN \gg 1$ and perform projection measurement of $|\psi_0(\infty)\rangle = |N/2, N/2\rangle_X$, and implement sudden quench to h_0^x satisfying $h_0^x/JN \approx 1$. In this case, the operation time to satisfy the adiabatic condition can be shorter than the first approach, while the initial state becomes $|\psi_0(\infty)\rangle$, which is not the ground state but close to it as discussed later. In this paper, we consider the latter case. Note that $h^x/JN = 1$ is the critical point in the thermodynamic limit, and thus we cannot prepare the ground state by cooling because of small energy gap. The initial state $|\psi_0(\infty)\rangle$ is expanded by the set of the bases $\{|\psi_m(h_0^x)\rangle\}_{m=0}^{N/2}$ as

$$|\psi_0(\infty)\rangle = \sum_{m=0}^{N/2} g_m |\psi_m(h_0^x)\rangle, \quad (14)$$

where $g_m = \langle \psi_m(h_0^x) | \psi_0(\infty) \rangle$.

The transverse field h^x is changed from h_0^x to 0 with finite operation time T_a . We express the time evolution operator of this process as \hat{U}_1 . The state after this process is

$$\hat{U}_1 |\psi_0(\infty)\rangle = \sum_{m,n=0}^{N/2} g_m g_{m \rightarrow n} |\psi_n(0)\rangle, \quad (15)$$

where $g_{m \rightarrow n} = \langle \psi_n(0) | \hat{U}_1 | \psi_m(h_0^x) \rangle$.

In the sensing process, the system is exposed to the target longitudinal field for a time interval T_{int} and each level rotates at different speed, i.e.,

$$e^{-i(\hat{\mathcal{H}} + \hat{V})T_{\text{int}}} \hat{U}_1 |\psi_0(\infty)\rangle = \sum_{m,n=0}^{N/2} g_m g_{m \rightarrow n} e^{iJ(N-2n)^2 T_{\text{int}}/2} \{ \cos[h^z(N-2n)T_{\text{int}}] |\psi_n(0)\rangle + i \sin[h^z(N-2n)T_{\text{int}}] |\phi_n(0)\rangle \}. \quad (16)$$

After the sensing process, we again change the transverse field h^x from 0 to h_0^x with the time T_a . We express the time evolution operator of this process as \hat{U}_2 . We then obtain the probe state

$$\begin{aligned} |\Psi_{T_{\text{int}}}(h^z)\rangle &= \hat{U}_2 e^{-i(\hat{\mathcal{H}} + \hat{V})T_{\text{int}}} \hat{U}_1 |\psi_0(\infty)\rangle \\ &= \sum_{m,n,l=0}^{N/2} g_m g_{m \rightarrow n} e^{iJ(N-2n)^2 T_{\text{int}}/2} \{ g_{n \rightarrow l}^\psi \cos[h^z(N-2n)T_{\text{int}}] |\psi_l(h_0^x)\rangle + i g_{n \rightarrow l}^\phi \sin[h^z(N-2n)T_{\text{int}}] |\phi_l(h_0^x)\rangle \}, \end{aligned} \quad (17)$$

where $g_{n \rightarrow l}^{\psi(\phi)} = \langle \psi_l(\phi_l)(h_0^x) | \hat{U}_2 | \psi_n(\phi_n)(0) \rangle$. The total operation time of the entire protocol is $T = 2T_a + T_{\text{int}}$.

Finally we perform the projection measurement of $|\psi_0(\infty)\rangle = |N/2, N/2\rangle_X$ and obtain

$$P = \left| \sum_{m,n,l=0}^{N/2} g_m g_{m \rightarrow n} g_{n \rightarrow l}^\psi g_l^* e^{iJ(N-2n)^2 T_{\text{int}}/2} \cos[h^z(N-2n)T_{\text{int}}] \right|^2 \quad (18)$$

as the survival probability of this measurement.

When the adiabatic condition is satisfied, i.e., when $g_{m \rightarrow n}^{(\psi)} = \delta_{mn} e^{i\alpha_m^{(\psi)}}$ holds with a phase factor $e^{i\alpha_m^{(\psi)}}$, we can provide a sufficient condition for achieving the Heisenberg limit scaling. The uncertainty of estimation (1) is bounded as

$$\delta h^z \leq \frac{1}{2NT_{\text{int}}(2|g_0|^4 - 1) \sin(2h^z NT_{\text{int}})} \quad (19)$$

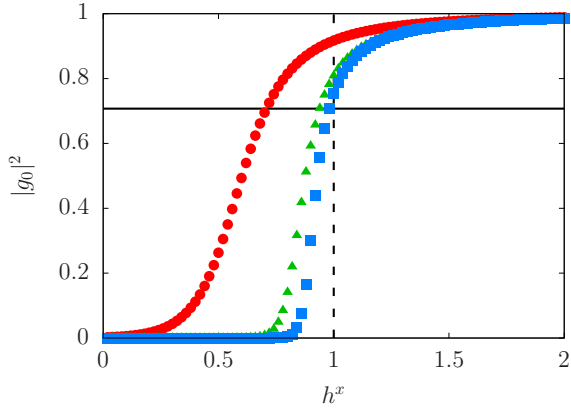


FIG. 1. Overlap between the initial state and the ground state $|g_0|^2 = |\langle \psi_0(h^x) | \psi_0(\infty) \rangle|^2$. The horizontal axis is the transverse field h^x in units of JN . Here, (red circles) $N = 10$, (green triangles) $N = 50$, and (blue squares) $N = 100$. The solid horizontal line represents the threshold $|g_0|^4 = 1/2$ and the dashed vertical line represents the critical point.

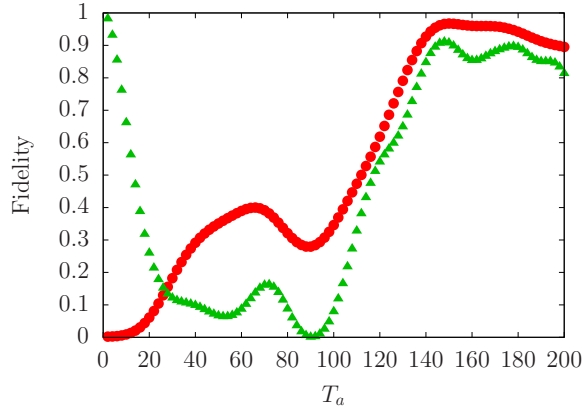


FIG. 2. Fidelity to the GHZ state at time $t = T_a$ (red circles) and to the initial state at time $t = 2T_a + T_{\text{int}} = 2T_a$ (green triangles) for $N = 10$. The horizontal axis is the operation time T_a in units of $(2JN^2)^{-1}$.

for $|g_0|^4 > 1/2$ when the condition $0 \leq 2h^z NT_{\text{int}} \leq \pi/2$ is satisfied (see, Appendix A, for derivation). Notably, the factor $\sin(2h^z NT_{\text{int}})$ becomes unity when we consider the phase shift discussed in Sec. II D and the right-hand side of Eq. (19) exactly coincides with the Heisenberg limit when $|g_0|^2 = 1$. This bound guarantees the Heisenberg limit scaling when the overlap between the initial state and the ground state, $|g_0|^2 = |\langle \psi_0(h_0^x) | \psi_0(\infty) \rangle|^2$, satisfies $|g_0|^4 > 1/2$, or rigorously $2|g_0|^4 - 1 = \Theta(N^0)$. We plot the overlap $|g_0|^2$ and the threshold $|g_0|^4 = 1/2$ in Fig. 1. We find that the initial condition $h_0^x = JN$ would be enough to achieve the Heisenberg limit scaling when $N \leq 100$ and provides shorter operation time T_a .

III. NUMERICAL SIMULATION

In this paper, we set $h_0^x = JN$ and change the transverse field h^x as $h^x = h_0^x \cos(\pi t/2T_a)$ for $0 \leq t \leq T_a$, which was introduced as coherent driving in Ref. [37] and is similar to a geometrically optimal schedule [39]. Under this transverse field, we can shorten the operation time T_a because nonadiabatic transitions and interference result in high fidelity to the GHZ state even in nonadiabatic time scale [37]. We also change the transverse field h^x as $h^x = h_0^x \sin\{\pi[t - (T_a + T_{\text{int}})]/2T_a\}$ for $T_a + T_{\text{int}} \leq t \leq 2T_a + T_{\text{int}}$. In the following numerical simulations, we set $JN = 1$.

First, we optimize the operation time T_a for the sensing time $T_{\text{int}} = 0$. We plot (red circles) the fidelity of the probe state to the GHZ state $|\psi_0(0)\rangle$ at the time $t = T_a$, i.e., $|\langle \psi_0(0) | \hat{U}_1 | \psi_0(\infty) \rangle|^2$, and (green triangles) that to the initial state $|\psi_0(\infty)\rangle$ at the time $t = 2T_a + T_{\text{int}} = 2T_a$, i.e., $|\langle \psi_0(\infty) | \hat{U}_2 \hat{U}_1 | \psi_0(\infty) \rangle|^2$, for $N = 10$ in Fig. 2. Here, interference appears when nonadiabatic transitions take place, and thus these quantities show oscillating behavior. We find a locally optimal operation time $T_a \approx 150(2JN^2)^{-1}$ showing high fidelity to the GHZ state (~ 0.97) and to the initial state (~ 0.91). Notably, it satisfies

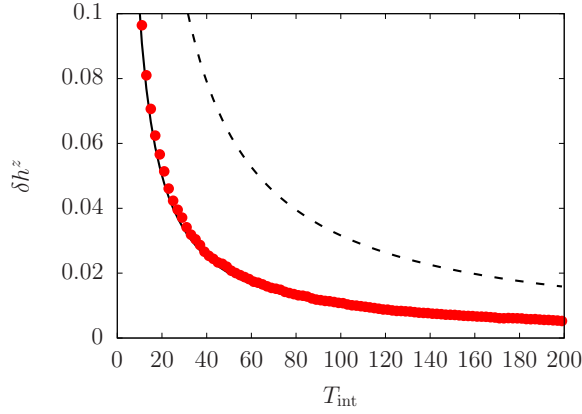


FIG. 3. Uncertainty of the estimation for $N = 10$. The horizontal axis is the sensing time T_{int} in units of $(2JN^2)^{-1}$ and the vertical axis is the uncertainty of estimation δh^z in units of JN . The solid and dashed curves represent the Heisenberg limit, $\delta h^z = 1/2NT_{\text{int}}$, and the SQL, $\delta h^z = 1/2N^{1/2}T_{\text{int}}$, respectively.

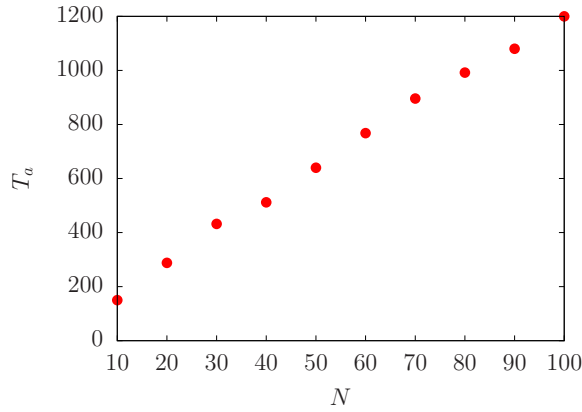


FIG. 4. Some examples of locally optimal operation time T_a with respect to the system size N . The vertical axis is in units of $(2JN^2)^{-1}$.

$g_{m \rightarrow n}^{(\psi)} \approx \delta_{mn} e^{i\alpha_m^{(\psi)}}$ because of interference although this locally optimal operation time is in nonadiabatic time scale.

Now, we set $T_a = 150(2JN^2)^{-1}$ and study the uncertainty of the estimation (1) for the infinitesimal target parameter h_u^z with the phase shift discussed in Sec. II D. We calculate the denominator of Eq. (1) by finite difference, $\partial P/\partial h_u^z \approx (P|_{h_u^z=10^{-10}} - P|_{h_u^z=0})/10^{-10}$. The sensing time T_{int} contributes to relative phases between different levels, and it affects the uncertainty of the estimation (1) [see, Eq. (18)]. Therefore, we plot the uncertainty of the estimation (1) with respect to T_{int} in Fig. 3. We find that the uncertainty is very close to the Heisenberg limit. Indeed, the uncertainty of the estimation (1) achieves $\delta h^z \approx 1.07/2NT_{\text{int}}$ on average for $(2JN^2)T_{\text{int}} = 1, 3, 5, \dots, 199$. Here, $(h_k^z + h_0^z)/JN = \pi/2$. Note that $1.07 \approx (0.93)^{-1}$ and thus it is smaller than that expected from the fidelity to the GHZ state (~ 0.97) and a little bit larger than that expected from the fidelity to the initial state (~ 0.91) for $T_{\text{int}} = 0$.

We also discuss these quantities for other system size, $N = 20, 30, 40, \dots, 100$. Some examples of locally optimal operation time are plotted with respect to system size N in Fig. 4. By using these locally optimal operation time, we calculate the uncertainty for several N against T_{int} (see Appendix B). We find that the uncertainty has some dependence on T_{int} and it slightly deviates from the Heisenberg limit. We express the average uncertainty of estimation as $\delta h^z = 1/2pNT_{\text{int}}$, where p ($0 \leq p \leq 1$) is an index denoting how close the uncertainty is to the Heisenberg limit. Here, the uncertainty is averaged for $(2JN^2)T_{\text{int}} = 1, 3, 5, \dots, 199$. For locally optimal time T_a in Fig. 4, the fidelity to the GHZ state (red circles), that to the initial state (green triangles), and the index p (blue squares) are calculated and plotted in Fig. 5. These quantities show complicated behavior against the number of qubits because of nonadiabatic transitions and interference. Remarkably, the uncertainty surpasses the SQL. Note that the shown performance is not the best, there exists other longer operation time showing better performance. If coherent time is long enough, we can choose those operation time.

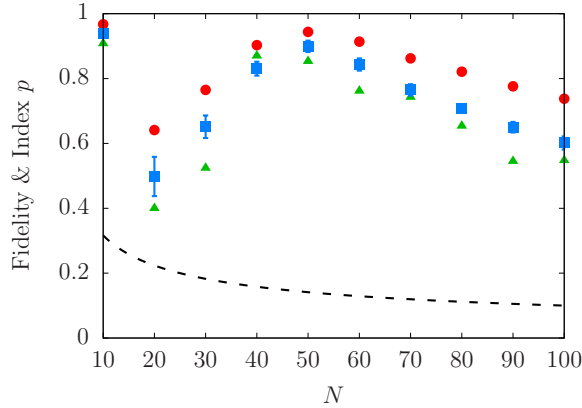


FIG. 5. System size dependence of (red circles) the fidelity of the probe state at time $t = T_a$ to the GHZ state, (green triangles) that of the probe state at time $t = 2T_a$ with $T_{\text{int}} = 0$ to the initial state, and (blue squares) the index p , which shows how close the uncertainty is to the Heisenberg limit on average. Here we use locally optimal time T_a plotted in Fig. 4. The error bar in the index p represents standard deviation and the dotted curve represents the SQL.

IV. DISCUSSION

First, we summarize the present paper. We proposed symmetry-protected adiabatic quantum metrology. In this protocol, parity measurement, which is difficult to be implemented in the experiments, is replaced with simple global magnetization measurement by adiabatic transformation of the transverse field. Here, we exploited the fact that the parity is a conserved quantity because of the spin-flip symmetry. We also discussed performance of our method in the realistic situations.

Next, we compare our method with other schemes. Replacing parity measurement with global magnetization measurement was also discussed in Ref. [10], where the one-axis twisting operation $U_{\text{OAT}} = \exp(i\pi\hat{S}_X^2/2)$ was used. In this case, the operation time is $(\pi/2)(2J)^{-1} = \mathcal{O}(J^{-1})$. As found in Fig. 4, the operation time of our scheme can be $\sim (11.6N + 60.0)(2JN^2)^{-1} = \mathcal{O}(J^{-1}N^{-1})$. Therefore, our scheme is faster than that in Ref. [10]. Our scheme is also more advantageous compared with the quantum domino dynamics-based scheme discussed in Ref. [34]. Although interactions are not necessarily turned off in their scheme as is also the case for ours, the operation time is $\mathcal{O}(N)$ in their scheme. Typically, the interaction strength J can be $\mathcal{O}(N^{-1})$ [44], i.e., the operation time of our scheme can be $\mathcal{O}(J^{-1}N^{-1}) = \mathcal{O}(N^0)$, and thus our scheme is also faster than that in Ref. [34].

Finally, we remark on robustness of our scheme. In this paper, we considered the finite transverse field and nonadiabatic transitions as possible errors in realistic situations. We leave effects of other errors and noises as future work, but we mention some evidence of robustness against various errors and noises. Our protocol utilizes the ground state, and thus decay from excited states to lower energy states during entanglement generation is less problematic than conventional dynamical approaches. In addition, the offset discussed in Sec. II D makes our protocol robust against measurement imperfection. Robustness of dynamics against bias, which breaks symmetry-protected conservation laws, during symmetry-protected adiabatic transformation was discussed in Ref. [40]. Robustness of entanglement generation against a loss process, which breaks a symmetry-protected conservation law and confinement in subspace of the Hilbert space, during (super)adiabatic transformation was discussed in Ref. [38]. Symmetry-protected superadiabatic transformation [38, 45] based on shortcuts to adiabaticity [46] can also speedup the present protocol and reduce negative effects.

ACKNOWLEDGMENTS

This work was supported by JST PRESTO Grant No. JPMJPR1919, JST CREST Grant No. JPMJCR1774, and Leading Initiative for Excellent Young Researchers, MEXT, Japan. MT is supported by JSPS fellowship (JSPS KAKENHI Grant No. 20J01757).

Appendix A: Derivation of the bound (19)

When the adiabatic condition is satisfied, Eq. (18) is given by

$$\begin{aligned}
P &= \left| \sum_{n=0}^{N/2} |g_n|^2 e^{i\gamma_n} \cos[h^z(N-2n)T_{\text{int}}] \right|^2 \\
&= \sum_{m,n=0}^{N/2} |g_m g_n|^2 e^{i(\gamma_m - \gamma_n)} \cos[h^z(N-2m)T_{\text{int}}] \cos[h^z(N-2n)T_{\text{int}}] \\
&= \frac{1}{2} \sum_{m,n=0}^{N/2} |g_m g_n|^2 e^{i(\gamma_m - \gamma_n)} \{ \cos[2h^z(N-m-n)T_{\text{int}}] + \cos[2h^z(m-n)T_{\text{int}}] \}.
\end{aligned} \tag{A1}$$

Now we estimate the denominator of Eq. (1). By using the triangle inequality, we obtain

$$\begin{aligned}
\left| \frac{\partial P}{\partial h^z} \right| &= \left| \sum_{m,n=0}^{N/2} |g_m g_n|^2 e^{i(\gamma_m - \gamma_n)} \{ (N-m-n)T_{\text{int}} \sin[2h^z(N-m-n)T_{\text{int}}] + (m-n)T_{\text{int}} \sin[2h^z(m-n)T_{\text{int}}] \} \right| \\
&\geq |g_0|^4 N T_{\text{int}} |\sin(2h^z N T_{\text{int}})| \\
&\quad - \left| \sum_{m,n=0}^{N/2} (1 - \delta_{m0} \delta_{n0}) |g_m g_n|^2 e^{i(\gamma_m - \gamma_n)} \right. \\
&\quad \left. \times \{ (N-m-n)T_{\text{int}} \sin[2h^z(N-m-n)T_{\text{int}}] + (m-n)T_{\text{int}} \sin[2h^z(m-n)T_{\text{int}}] \} \right| \\
&\geq |g_0|^4 N T_{\text{int}} |\sin(2h^z N T_{\text{int}})| \\
&\quad - \sum_{m,n=0}^{N/2} (1 - \delta_{m0} \delta_{n0}) |g_m g_n|^2 |(N-m-n)T_{\text{int}} \sin[2h^z(N-m-n)T_{\text{int}}] + (m-n)T_{\text{int}} \sin[2h^z(m-n)T_{\text{int}}]| \\
&= |g_0|^4 N T_{\text{int}} |\sin(2h^z N T_{\text{int}})| \\
&\quad - \left(\sum_{m,n=1}^{N/2} \delta_{mn} + 2 \sum_{\substack{m,n=0 \\ (m>n)}}^{N/2} \right) |g_m g_n|^2 |(N-m-n)T_{\text{int}} \sin[2h^z(N-m-n)T_{\text{int}}] + (m-n)T_{\text{int}} \sin[2h^z(m-n)T_{\text{int}}]|.
\end{aligned} \tag{A2}$$

When the condition $0 \leq 2h^z N T_{\text{int}} \leq \pi/2$ is satisfied, the following inequalities hold:

$$0 \leq (N-m-n) \sin[2h^z(N-m-n)T_{\text{int}}] \leq (N-m) \sin(2h^z N T_{\text{int}}) \tag{A3}$$

and

$$0 \leq (m-n) \sin[2h^z(m-n)T_{\text{int}}] \leq m \sin(2h^z N T_{\text{int}}) \tag{A4}$$

for $0 \leq m, n \leq N/2$ and $m \geq n$. Therefore, we obtain

$$\begin{aligned}
&\left(\sum_{m,n=1}^{N/2} \delta_{mn} + 2 \sum_{\substack{m,n=0 \\ (m>n)}}^{N/2} \right) |g_m g_n|^2 |(N-m-n)T_{\text{int}} \sin[2h^z(N-m-n)T_{\text{int}}] + (m-n)T_{\text{int}} \sin[2h^z(m-n)T_{\text{int}}]| \\
&\leq \left(\sum_{m,n=1}^{N/2} \delta_{mn} + 2 \sum_{\substack{m,n=0 \\ (m>n)}}^{N/2} \right) |g_m g_n|^2 N \sin(2h^z N T_{\text{int}}).
\end{aligned} \tag{A5}$$

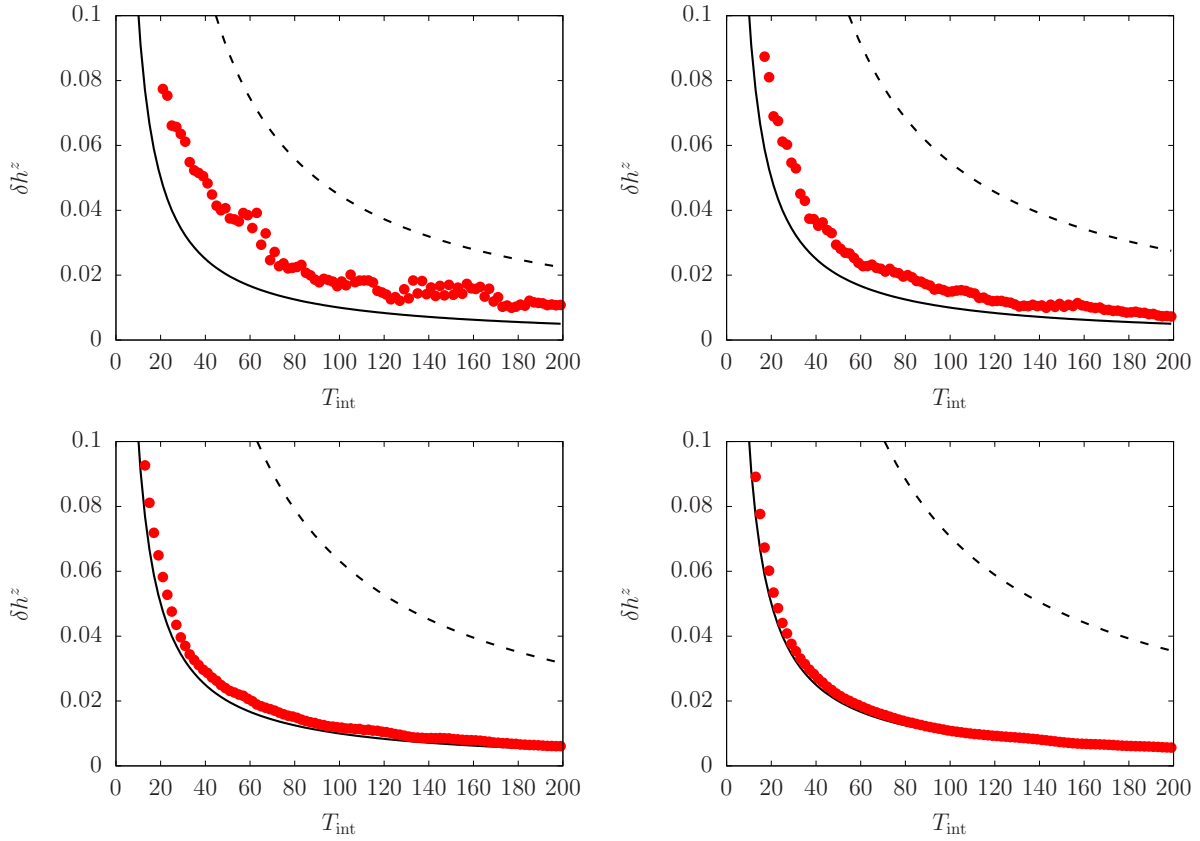


FIG. 6. Uncertainty of the estimation for (top left) $N = 20$, (top right) $N = 30$, (bottom left) $N = 40$, and (bottom right) $N = 50$. The horizontal axis is the sensing time T_{int} in units of $(2JN^2)^{-1}$ and the vertical axis is the uncertainty of estimation δh^z in units of JN . The solid and dashed curves represent the Heisenberg limit, $\delta h^z = 1/2NT_{\text{int}}$, and the SQL, $\delta h^z = 1/2N^{1/2}T_{\text{int}}$, respectively.

Moreover, we find

$$\left(\sum_{m,n=1}^{N/2} \delta_{mn} + 2 \sum_{\substack{m,n=0 \\ (m>n)}}^{N/2} \right) |g_m g_n|^2 = \sum_{m,n=0}^{N/2} (1 - \delta_{m0} \delta_{n0}) |g_m g_n|^2 = 1 - |g_0|^4. \quad (\text{A6})$$

Finally we obtain

$$\left| \frac{\partial P}{\partial h^z} \right| \geq NT_{\text{int}}(2|g_0|^4 - 1) \sin(2h^z NT_{\text{int}}) \quad (\text{A7})$$

for $|g_0|^4 > 1/2$. For $|g_0|^4 \leq 1/2$, we use $|\partial P/\partial h^z| \geq 0$ and it results in a trivial bound $\delta h^z \leq \infty$.

Together with a trivial inequality $\sqrt{P(1-P)} \leq 1/2$, we find a bound for the uncertainty of estimation (19)

$$\delta h^z \leq \frac{1}{2NT_{\text{int}}(2|g_0|^4 - 1) \sin(2h^z NT_{\text{int}})} \quad (\text{A8})$$

for $|g_0|^4 \geq 1/2$. This is the derivation of the bound (19).

Appendix B: Other system size

Similarly to the case for $N = 10$ in Sec. III, we also calculate the uncertainty of the estimation for $N = 20, 30, 40$, and 50 against the sensing time T_{int} in Fig. 6, as examples. We find that, depending on system size, dependence of the uncertainty on

the sensing time T_{int} is not negligible. Therefore, we discuss the uncertainty of the estimation averaged over the sensing time T_{int} in the main text.

[1] G. Tóth and I. Apellaniz, Quantum metrology from a quantum information science perspective, *Journal of Physics A: Mathematical and Theoretical* **47**, 424006 (2014).

[2] C. L. Degen, F. Reinhard, and P. Cappellaro, Quantum sensing, *Reviews of Modern Physics* **89**, 035002 (2017).

[3] L. Pezzè, A. Smerzi, M. K. Oberthaler, R. Schmied, and P. Treutlein, Quantum metrology with nonclassical states of atomic ensembles, *Reviews of Modern Physics* **90**, 035005 (2018).

[4] C. M. Caves, Quantum-mechanical noise in an interferometer, *Physical Review D* **23**, 1693 (1981).

[5] V. Giovannetti, S. Lloyd, and L. Maccone, Quantum-enhanced measurements: beating the standard quantum limit., *Science* **306**, 1330 (2004).

[6] V. Giovannetti, S. Lloyd, and L. Maccone, Quantum Metrology, *Physical Review Letters* **96**, 010401 (2006).

[7] D. M. Greenberger, M. A. Horne, A. Shimony, and A. Zeilinger, Bell's theorem without inequalities, *American Journal of Physics* **58**, 1131 (1990).

[8] N. D. Mermin, Extreme quantum entanglement in a superposition of macroscopically distinct states, *Physical Review Letters* **65**, 1838 (1990).

[9] J. J. Bollinger, W. M. Itano, D. J. Wineland, and D. J. Heinzen, Optimal frequency measurements with maximally correlated states, *Physical Review A* **54**, R4649 (1996).

[10] D. Leibfried, M. D. Barrett, T. Schaetz, J. Britton, J. Chiaverini, W. M. Itano, J. D. Jost, C. Langer, and D. J. Wineland, Toward Heisenberg-Limited Spectroscopy with Multiparticle Entangled States, *Science* **304**, 1476 (2004).

[11] Y. Matsuzaki, S. C. Benjamin, and J. Fitzsimons, Magnetic field sensing beyond the standard quantum limit under the effect of decoherence, *Physical Review A* **84**, 012103 (2011).

[12] A. W. Chin, S. F. Huelga, and M. B. Plenio, Quantum Metrology in Non-Markovian Environments, *Physical Review Letters* **109**, 233601 (2012).

[13] R. Chaves, J. B. Brask, M. Markiewicz, J. Kołodyński, and A. Acín, Noisy Metrology beyond the Standard Quantum Limit, *Physical Review Letters* **111**, 120401 (2013).

[14] W. Dür, M. Skotiniotis, F. Fröwis, and B. Kraus, Improved Quantum Metrology Using Quantum Error Correction, *Physical Review Letters* **112**, 080801 (2014).

[15] K. Macieszczak, Zeno limit in frequency estimation with non-Markovian environments, *Physical Review A* **92**, 010102 (2015).

[16] S. Zhou, M. Zhang, J. Preskill, and L. Jiang, Achieving the Heisenberg limit in quantum metrology using quantum error correction, *Nature Communications* **9**, 78 (2018).

[17] Y. Matsuzaki, S. Benjamin, S. Nakayama, S. Saito, and W. J. Munro, Quantum Metrology beyond the Classical Limit under the Effect of Dephasing, *Physical Review Letters* **120**, 140501 (2018).

[18] D. Leibfried, E. Knill, S. Seidelin, J. Britton, R. B. Blakestad, J. Chiaverini, D. B. Hume, W. M. Itano, J. D. Jost, C. Langer, R. Ozeri, R. Reichle, and D. J. Wineland, Creation of a six-atom ‘Schrödinger cat’ state, *Nature* **438**, 639 (2005).

[19] P. Neumann, N. Mizuochi, F. Rempp, P. Hemmer, H. Watanabe, S. Yamasaki, V. Jacques, T. Gaebel, F. Jelezko, and J. Wrachtrup, Multipartite Entanglement Among Single Spins in Diamond, *Science* **320**, 1326 (2008).

[20] J. A. Jones, S. D. Karlen, J. Fitzsimons, A. Ardavan, S. C. Benjamin, G. A. D. Briggs, and J. J. L. Morton, Magnetic field sensing beyond the standard quantum limit using 10-spin NOON states., *Science* **324**, 1166 (2009).

[21] L. DiCarlo, M. D. Reed, L. Sun, B. R. Johnson, J. M. Chow, J. M. Gambetta, L. Frunzio, S. M. Girvin, M. H. Devoret, and R. J. Schoelkopf, Preparation and measurement of three-qubit entanglement in a superconducting circuit, *Nature* **467**, 574 (2010).

[22] M. Neeley, R. C. Bialczak, M. Lenander, E. Lucero, M. Mariantoni, A. D. O’Connell, D. Sank, H. Wang, M. Weides, J. Wenner, Y. Yin, T. Yamamoto, A. N. Cleland, and J. M. Martinis, Generation of three-qubit entangled states using superconducting phase qubits, *Nature* **467**, 570 (2010).

[23] R. Barends, J. Kelly, A. Megrant, A. Veitia, D. Sank, E. Jeffrey, T. C. White, J. Mutus, A. G. Fowler, B. Campbell, Y. Chen, Z. Chen, B. Chiaro, A. Dunsworth, C. Neill, P. O’Malley, P. Roushan, A. Vainsencher, J. Wenner, A. N. Korotkov, A. N. Cleland, and J. M. Martinis, Superconducting quantum circuits at the surface code threshold for fault tolerance, *Nature* **508**, 500 (2014).

[24] K. X. Wei, I. Lauer, S. Srinivasan, N. Sundaresan, D. T. McClure, D. Toyli, D. C. McKay, J. M. Gambetta, and S. Sheldon, Verifying multipartite entangled Greenberger-Horne-Zeilinger states via multiple quantum coherences, *Physical Review A* **101**, 032343 (2020).

[25] M. Kitagawa and M. Ueda, Squeezed spin states, *Physical Review A* **47**, 5138 (1993).

[26] G. Agarwal, R. Puri, and R. Singh, Atomic Schrödinger cat states, *Physical Review A* **56**, 2249 (1997).

[27] K. Mølmer and A. Sørensen, Multipartite Entanglement of Hot Trapped Ions, *Physical Review Letters* **82**, 1835 (1999).

[28] S. M. Chumakov, A. Frank, and K. B. Wolf, Finite Kerr medium: Macroscopic quantum superposition states and Wigner functions on the sphere, *Physical Review A* **60**, 1817 (1999).

[29] A. Micheli, D. Jaksch, J. I. Cirac, and P. Zoller, Many-particle entanglement in two-component Bose-Einstein condensates, *Physical Review A* **67**, 013607 (2003).

[30] L. Pezzè and A. Smerzi, Entanglement, Nonlinear Dynamics, and the Heisenberg Limit, *Physical Review Letters* **102**, 100401 (2009).

[31] C. Song, K. Xu, W. Liu, C.-p. Yang, S.-B. Zheng, H. Deng, Q. Xie, K. Huang, Q. Guo, L. Zhang, P. Zhang, D. Xu, D. Zheng, X. Zhu, H. Wang, Y.-A. Chen, C.-Y. Lu, S. Han, and J.-W. Pan, 10-Qubit Entanglement and Parallel Logic Operations with a Superconducting Circuit, *Physical Review Letters* **119**, 180511 (2017).

- [32] C. Song, K. Xu, H. Li, Y.-R. Zhang, X. Zhang, W. Liu, Q. Guo, Z. Wang, W. Ren, J. Hao, H. Feng, H. Fan, D. Zheng, D.-W. Wang, H. Wang, and S.-Y. Zhu, Generation of multicomponent atomic Schrödinger cat states of up to 20 qubits, *Science* **365**, 574 (2019).
- [33] P. A. Ivanov and D. Porras, Adiabatic quantum metrology with strongly correlated quantum optical systems, *Physical Review A* **88**, 023803 (2013).
- [34] A. Yoshinaga, M. Tatsuta, and Y. Matsuzaki, Entanglement-enhanced sensing with an always-on nearest-neighbor interaction between qubits, (2021), arXiv:2101.02998.
- [35] J. I. Cirac, M. Lewenstein, K. Mølmer, and P. Zoller, Quantum superposition states of Bose-Einstein condensates, *Physical Review A* **57**, 1208 (1998).
- [36] C. Lee, Adiabatic Mach-Zehnder Interferometry on a Quantized Bose-Josephson Junction, *Physical Review Letters* **97**, 150402 (2006).
- [37] E. Yukawa, G. J. Milburn, and K. Nemoto, Fast macroscopic-superposition-state generation by coherent driving, *Physical Review A* **97**, 013820 (2018).
- [38] T. Hatomura and K. Pawłowski, Superadiabatic generation of cat states in bosonic Josephson junctions under particle losses, *Physical Review A* **99**, 043621 (2019).
- [39] T. Hatomura, Suppressing nonadiabatic transitions during adiabatic generation of highly entangled states in bosonic Josephson junctions, *Physical Review A* **100**, 043619 (2019).
- [40] M. Zhuang, J. Huang, Y. Ke, and C. Lee, Symmetry-Protected Quantum Adiabatic Evolution in Spontaneous Symmetry-Breaking Transitions, *Annalen der Physik* **532**, 1900471 (2020).
- [41] S. Endo, Y. Matsuzaki, K. Kakuyanagi, S. Saito, N. Lambert, and F. Nori, Projecting an ultra-strongly-coupled system in a non-energy-eigenbasis with a driven nonlinear resonator, *Scientific Reports* **10**, 1751 (2020).
- [42] J. M. Taylor, P. Cappellaro, L. Childress, L. Jiang, D. Budker, P. R. Hemmer, A. Yacoby, R. Walsworth, and M. D. Lukin, High-sensitivity diamond magnetometer with nanoscale resolution, *Nature Physics* **4**, 810 (2008).
- [43] S. Kitazawa, Y. Matsuzaki, S. Saito, K. Kakuyanagi, S. Saito, and J. Ishi-Hayase, Vector-magnetic-field sensing via multifrequency control of nitrogen-vacancy centers in diamond, *Physical Review A* **96**, 042115 (2017).
- [44] S. Dooley, E. Yukawa, Y. Matsuzaki, G. C. Knee, W. J. Munro, and K. Nemoto, A hybrid-systems approach to spin squeezing using a highly dissipative ancillary system, *New Journal of Physics* **18**, 053011 (2016).
- [45] T. Hatomura, Shortcuts to adiabatic cat-state generation in bosonic Josephson junctions, *New Journal of Physics* **20**, 015010 (2018).
- [46] D. Guéry-Odelin, A. Ruschhaupt, A. Kiely, E. Torrontegui, S. Martínez-Garaot, and J. G. Muga, Shortcuts to adiabaticity: Concepts, methods, and applications, *Reviews of Modern Physics* **91**, 045001 (2019).